Electronic structure of icosahedral $Al_{70}Pd_{20}Mn_{10}$

G. W. Zhang and Z. M. Stadnik*
Department of Physics, University of Ottawa, Ottawa, Ontario, Canada K1N 6N5

A.-P. Tsai and A. Inoue
Institute for Materials Research, Tohoku University, Sendai 980, Japan
(Received 17 February 1994; revised manuscript received 13 May 1994)

Photoemission spectroscopy measurements in the photon-energy range 35–150 eV have been used to determine the valence band of the stable icosahedral alloy $Al_{70}Pd_{20}Mn_{10}$. Resonant photoemission near the Mn $3p \rightarrow 3d$ transition has been employed to show that the feature in the valence band at about 1.0 eV below the Fermi level is predominantly due to the Mn $3d$-derived states. The effect of the Cooper minimum has been used to identify the feature at 3.6 eV below the Fermi level as being mainly due to states of Pd $4d$ character. The strong decrease of intensity towards the Fermi level has been interpreted as indicative of the presence of a pseudogap at the Fermi level. However, it is shown that the Fermi cutoff also contributes to the observed intensity decrease. No unusual features in the valence band of icosahedral $Al_{70}Pd_{20}Mn_{10}$ which could be ascribed to its quasiperiodic nature have been observed within the experimental resolution. A review of published experimental results on the electronic structure of quasicrystals obtained with techniques directly probing the occupied and unoccupied electronic states is also presented.

I. INTRODUCTION

The dramatic discovery of an icosahedral Al-Mn alloy by Shechtman *et al.*[1] extended the dichotomous division of solids into either crystalline or amorphous by introducing the notion of quasicrystals (QC's). This new form of matter has long-range quasiperiodic order and long-range orientational order of crystallographically forbidden (fivefold, eightfold, tenfold, and 12-fold) symmetries.[2] A central problem in solid-state physics is to determine whether this quasiperiodic structure leads to physical properties which are found neither in crystalline nor in amorphous materials.

Prior to 1987, all known QC's were thermodynamically *metastable.* They exhibited significant structural disorder as manifested in the broadening of the x-ray-diffraction lines and it was argued that this disorder might inhibit detecting possible intrinsic physical properties. Experiments conducted on such QC's showed that their physical properties are quite similar to those corresponding to crystalline or amorphous alloys.[2,3]

It was therefore of great importance when the first thermodynamically stable icosahedral (i) alloys Al-Cu-M (M = Fe, Ru, Os) were discovered[4] since they possess a high degree of structural perfection comparable to that found in the best periodic alloys. Indeed these i alloys exhibit some unusual behavior.[3] Their most striking characteristics, which are not expected for compounds formed of normal metallic elements, are the very high resistivities (up to 0.01 Ω cm in Al-Cu-Fe alloys at 4.2 K,[3] up to 0.03 Ω cm in Al-Cu-Ru alloys,[3] and up to the record high value of 0.28 Ω cm in Al-Pd-Re alloys[5,6]), and temperature coefficients which are generally negative. This puts them at the border of the metal-insulator transition. It was suggested in a recent experimental study[5] that i-Al-Pd-Re alloys are in fact quasiperiodic insulators. The resistivity of these i alloys depends on the structural quality of the sample used in a very peculiar way; it increases when the structural defects are removed,[7] which is at variance with the behavior of typical metals. Furthermore, the resistivity is extremely sensitive to sample composition,[6,7] which is reminiscent of doping effects in semiconductors. Other anomalies in transport properties of QC's, such as low electronic contribution to the specific heat, large and strongly temperature-dependent Hall coefficients and thermoelectric power, or a non-Drude-like optical conductivity, have also been observed and are reviewed in Ref. 3.

The anomalously high resistivity has been attributed[7,8] to a very low density of states at the Fermi level, DOS(E_F), rather than to a short mean free path. The low DOS(E_F), in turn, may be a consequence of a Hume-Rothery stabilization mechanism, which is believed to occur in QC's, and which places the Fermi level into a minimum of DOS. The existence of a pseudogap at E_F was also predicted by theory based on the nearly free-electron approximation[9] and by the electronic structure calculations for the lowest-order crystalline approximants.[10]

The low-temperature and magnetic-field dependencies of this high resistivity have been analyzed[7,11,12] with quantum interference theories (weak localization and electron-electron interaction). Such theories, however, were originally developed for highly disordered conductors. Thus, their apparent relevance to QC's suggests that QC's are electronically disordered alloys. This, however, poses a question which has yet to be answered: how can such electronic disorder be reconciled with the apparent high degree of local atomic order, as determined by diffraction and electron-microscopy experiments, in stable QC's?

Recently, a stable i phase has been found in the Al-Pd-Mn system.[13] It differs from other stable i phases in that the samples are free of atomic disorder and phason strains even in the rapidly solidified state.[14] Furthermore, this phase forms in a wide composition range.

Structural studies with different techniques show that this phase forms in a perfect *i* state.[15–18] Therefore, this system is ideal for studies of its possible unusual physical properties.

Most of the studies performed so far are related to various structural aspects of the *i*-Al-Pd-Mn alloys investigated by x-ray and neutron diffraction,[15,16] extended x-ray absorption fine-structure (EXAFS),[17] and various electron microscopy techniques.[18] The recent investigations of their physical properties are briefly reviewed below.

The first magnetic measurements[19] indicated distinct differences in the magnetic properties between *i* and corresponding amorphous alloys in the Al-Pd-Mn system. Spin-glass behavior was observed in *i*-Al-Pd-Mn alloys and the data were interpreted in terms of magnetic and nonmagnetic Mn atoms.[19] Furthermore, the concept of a giant magnetic moment on the Mn atoms was invoked,[19] which is also known to exist in crystalline alloys of transition metals in a Pd matrix. Recent magnetic studies of the *i*-Al-Pd-Mn alloys[20] show the presence of both diamagnetic and paramagnetic susceptibilities. The alloys seem to become more diamagnetic as their resistivity increases.[20] An anisotropy in the nonlinear region of the magnetization versus magnetic field curve along the five-, three-, and twofold axes was found recently[21] in a single-grained *i*-$Al_{68}Pd_{23}Mn_9$. In the very recent magnetic study of the *i*-$Al_{70}Pd_{21}Mn_9$ alloy[22] a spin-glass-like maximum at 0.5 K was observed and a very low concentration of Mn magnetic moments (1.2% of all Mn atoms) involved in the spin-glass transition was found. It was indicated that the frustration of magnetic moments plays an important role in forming a spin-glass state in *i*-$Al_{70}Pd_{21}Mn_9$. It could be added that a high degree of magnetic frustration is most probably the consequence of an inherent disorder present even in the most perfect (as determined by diffraction or electron-microscopy techniques) *i* systems, and which can be clearly detected by local probes, such as NMR or Mössbauer spectroscopy (for a recent review of Mössbauer studies, see Ref. 23). Early theoretical calculations[24] based on the multiple-scattering X-α technique applied to small Al-Mn clusters predicted that Mn sites in Al-Mn-based *i* alloys should carry a magnetic moment, which was taken to imply[24,25] that the *i* symmetry is responsible for the formation of a magnetic moment at the Mn sites. It has been recently shown in a convincing way[26] that this conclusion[24,25] is based on an artifact of the small cluster used to mimic the solid[24,25] and that, in reality, this moment is quenched for a larger size of the cluster.[26] One can thus argue[27] that the presence of the nonzero Mn moment observed experimentally in thermodynamically stable and metastable *i* alloys is due, at least partially, to the inherent chemical disorder in the transition-metal sublattice present in all QC's with transition-metal elements.[23]

NMR measurements[28] have been interpreted in terms of two classes of Mn sites invoked earlier to explain magnetic measurements.[19,20,22] Inelastic neutron-scattering experiments[29] indicate the presence of some fine structure in the generalized vibrational density of states which were not found previously in other stable *i* alloys. However, a conclusive interpretation of the experimental data is hampered by the lack of theoretical calculations based on realistic structural models. The self-diffusivity of Mn in *i*-$Al_{72}Pd_{20}Mn_8$ was found[30] to be about 2 orders of magnitude smaller than in crystalline $Al_{60}Pd_{25}Mn_{15}$ and about 3–4 orders of magnitude smaller than in crystalline Al; this interesting experimental result has yet to find an appropriate explanation. It is also interesting to notice that the *i*-Al-Pd-Mn alloys have potential for practical applications. It has been recently shown[31] that the room-temperature hardness of *i*-$Al_{72}Pd_{20}Mn_8$ is 86% larger than that of crystalline cubic $Al_{60}Pd_{25}Mn_{15}$.

Resistivities of up to 10 000 $\mu\Omega$ cm were found at low temperatures in the *i*-Al-Pd-Mn alloys.[12,20,32] It was also noted that the resistivity strongly depends on the composition and on the structural quality of the samples used.[20] An anisotropy of resistivity along the two-, three-, and fivefold axes was demonstrated for a single-grained *i*-$Al_{70}Pd_{20}Mn_{10}$.[32] The high values of resistivity were interpreted as evidence for the presence of a pseudogap in the electronic density of states at the Fermi level.[12,20] The presence of such a pseudogap has also been invoked in the interpretation of the optical conductivity data.[33] The resistivity temperature dependence was interpreted with the theory of the weak localization in a regime of strong spin-orbit scattering.[12] However, the magnetoresistance temperature dependence could not be explained by this theory.[12] A low value of DOS(E_F) is also expected from the low value of the electronic specific heat of *i*-Al-Pd-Mn alloys, which was found to be about three times smaller than that of Al metal.[12,22]

It thus seems that very high resistivities and diamagnetism are characteristic features of all stable *i* alloys of high structural quality. This, in turn, implies very low values of DOS(E_F), i.e., the possible presence of a pseudogap at E_F, which is also predicted by theory[9,10] (a brief review of different theoretical methods used to calculate the electronic structure of QC's is presented in Ref. 34). The theory also suggests[10] that the DOS has a dense and very spiky structure.

To determine experimentally any possible unusual features in the DOS of *i* alloys, and in particular the existence of a pseudogap around E_F, one needs information not only on the DOS(E_F), which is inferred *indirectly* from the specific heat and/or resistivity measurements,[3,34] but also on the DOS below and above E_F. Therefore, studies using spectroscopic techniques which probe DOS at energies in the vicinity of E_F are extremely useful. The DOS below E_F was studied with the x-ray photoelectron spectroscopy (XPS), photoemission spectroscopy (PES), and soft x-ray emission (SXE) spectroscopy, whereas the DOS above E_F was probed with the inverse photoemission spectroscopy (IPES) and soft x-ray-absorption (SXA) spectroscopy in Al-Mn-Si, Al-Li-Cu-Mg, Al-Cu-Fe-Cr, Al-Pd-Mn, and Al-Cu-Mn QC's.[34–47] These electronic structure studies lead to several conclusions, which will be discussed in detail in Sec. III in relation to the present study, and which are summarized below. First, the most important finding is the apparent observation of the theoretically predicted pseudogap at

E_F in some of the studied QC's. However, an unambiguous PES experimental verification of the existence of such a pseudogap for QC's containing the transition-metal (TM) elements is very difficult because the experimentally measured intensity in the vicinity of E_F is dominated by the TM 3*d* states, as is well known from the similar studies of the structurally induced minimum in the DOS in amorphous alloys.[48] Second, chemical shifts of the Al 2*p* lines are either zero or very small with respect to similar crystalline compounds or pure elements. This is at odds with the theoretical result[24] predicting large shifts (0.8 eV), and thus confirms the conclusion of other theoretical studies[26] of the unreliability of the theoretical predictions[24,25] based on calculations performed on small clusters. Third, a close structural similarity between the valence-band spectra of QC's and those of the corresponding crystalline compounds was found. No dense and sharp features in the DOS of QC's predicted by the theory were observed. Finally, various measured spectral features were ascribed to particular electronic states of *s*, *p*, and *d* character, and evidence of hybridization between *sp* and *d* states was presented.

The present study of the high structural quality, stable *i*-$Al_{70}Pd_{20}Mn_{10}$ alloy by the synchrotron-radiation-based PES technique was undertaken to determine its electronic structure. In particular, an attempt was made to reliably determine the origin of the features observed in the valence band and verify the possible existence of a pseudogap at the Fermi level.

II. EXPERIMENTAL PROCEDURE

An alloy of composition $Al_{70}Pd_{20}Mn_{10}$ was produced by arc melting high-purity elemental constituents in argon. It was annealed between 1123 and 1173 K for 10 h in vacuum, and then cut into slices suitable for PES measurements. The details of the sample preparation are described elsewhere.[5]

X-ray-diffraction (XRD) measurements on powder obtained from the slices of the $Al_{70}Pd_{20}Mn_{10}$ alloy chosen for PES studies were performed on a Philips X'Pert scanning diffractometer equipped with a PW3020 vertical goniometer with a 173-mm radius. This goniometer uses dc motors instead of conventional stepper motors and the Θ and 2Θ angles are monitored via two optical encoder disks mounted directly on a drive shaft. This allows the 2Θ accuracy of about 0.003° to be achieved. Corrections were made to the 2Θ angles to allow for the possible instrumental abberation and specimen displacement from the scan of the specimen mixed with 10 wt % of a Si standard reference material 640 b. The diffractometer was equipped with a variable divergence slit which kept the illuminated length of the sample constant at 12.5 mm, and a 0.1-mm receiving slit was used. With this setting the instrumental resolution, as determined from the full width at half maximum of the (111) peak of a Si standard, was 0.007 $Å^{-1}$. A fine sample powder was mixed with methanol and allowed to dry on a low-background sample holder cut from a single crystal of Si, resulting in a thin flat sample. A sample spinner was used to further minimize a possible preferred sample orientation. Cu $K\alpha$ radiation was employed and the $K\beta$ line was eliminated by using a Kevex PSi2 Peltier cooled Si detector.

Photoemission spectra were collected on beamline U14A at the National Synchrotron Light Source at Brookhaven National Laboratory. Photon energies between 35 and 150 eV were selected with a plane grating monochromator. The normal to the sample was at an angle of 45° to both the photon beam and the axis of a PHI 15-255 precision electron energy analyzer. The resulting overall resolution was 0.4 eV. The sample was cleaned in the experimental vacuum chamber either by Ar-ion bombardment or by mechanical abrasion using an alumina scraper. No differences between the PES spectra corresponding to these two surface-treatment methods could be detected. This is consistent with the observation that no significant change of the composition of the surface region, with respect to that of the bulk, occurs in Pd-containing alloys during Ar-ion bombardment.[49] The surface cleanliness of the sample was frequently checked by monitoring the appearance of the oxide features in the Al 2*p* line and/or in the valence band.[34] The base pressure in the experimental chamber was in the high 10^{11}-Torr range. No effects due to charge build up were observed during the PES experiments.

All the spectra presented in this work were obtained from at least two different regions of the sample studied, and turned out to be indistinguishable within the resolution of the experiment. The position of the Fermi level was determined with an accuracy of 0.05 eV by measuring the Fermi edge and/or the Al 2*p* line (for photon energies larger than 100 eV) of an adjacent Al sample. It was additionally verified by a linear extrapolation of the leading edge of the valence band of the measured spectra.

III. RESULTS AND DISCUSSION

A. X-ray diffraction data

The XRD spectrum of the studied sample measured in the 2Θ range 6°–123° (Fig. 1) shows the presence of many Bragg lines, the weaker of which are usually not observed in the spectra obtained with a scintillation detector. This increased sensitivity for weak lines is due to the solid-state detector which has a higher counting efficiency (due to the elimination of a monochromator in the diffracted beam) and lower background count rate as compared to a more conventional scintillation detector. The positions of all the detected Bragg lines corresponding to Cu $K\alpha_1$ radiation ($\lambda = 1.540\,598\,1$ Å) in terms of the angle $2\Theta_1$ and the corresponding wave number $Q_{\text{expt}} = 4\pi \sin\Theta_1/\lambda$, as well as their relative intensities and full widths at half maximum Γ_Q, were determined from the profile fitting using the procedure described by Schreiner and Jenkins.[50] These parameters corresponding to 61 detected *i* peaks, whose positions are indicated by the vertical lines in Fig. 1, are presented in Table I together with the calculated (taking the line number 17 as the reference line) line positions Q_{calc} and the corresponding indexes. Since there are several schemes employed to index the *i* lines, we present the indexes corresponding to most often used schemes[51–53] in order to enable the reader to make con-

venient identification of the *i* lines.

Most of the observed Bragg lines can be indexed to the *i* structure. It is noticeable that even the peaks with an intensity as small as 0.2% of the most intense peak could be detected and indexed to the *i* structure. There is excellent agreement between the observed Q_{expt} and theoretical Q_{calc} positions (Table I) of the peaks. Out of 61 detected *i* peaks, 60 are at the positions within ± 0.001 Å^{-1} and only one (peak number 53) within ± 0.002 Å^{-1} of the values calculated for the six-dimensional face-centered *i* lattice. The peak widths (Table I) are found to be limited by the instrumental resolution. The presence of the superlattice lines (Fig. 1 and Table I), for which N in the N/M index[51] is equal to $4n+3$ (the strongest superlattice line is the line number 7),[54] confirms[15,16] that *i*-$Al_{70}Pd_{20}Mn_{10}$ has the six-dimensional face-centered-cubic Bravais lattice. The value of the six-dimensional cubic lattice constant $a_{6D}=6.461$ Å is in a good agreement with values found in the literature.[15,16]

All other weak nonicosahedral Bragg peaks in Fig. 1, except three, could be identified with the peaks due to the presence of a small amount of the hexagonal Al_3Pd_2 (JCPDS file 6-0654) and decagonal Al_4Mn (JCPDS file 40-1080) alloys as the second phases. The presence of these alloys in the Al-Pd-Mn phase diagram has been observed earlier by electron microscopy techniques by Beeli *et al.* and Audier *et al.*[18] It is thus concluded that the studied sample is predominantly single phase *i* alloy.

B. Methodology of the correction of the photoemission spectroscopy data

In order to compare the intensities of the synchrotron-radiation-based PES spectra of a given sample, several

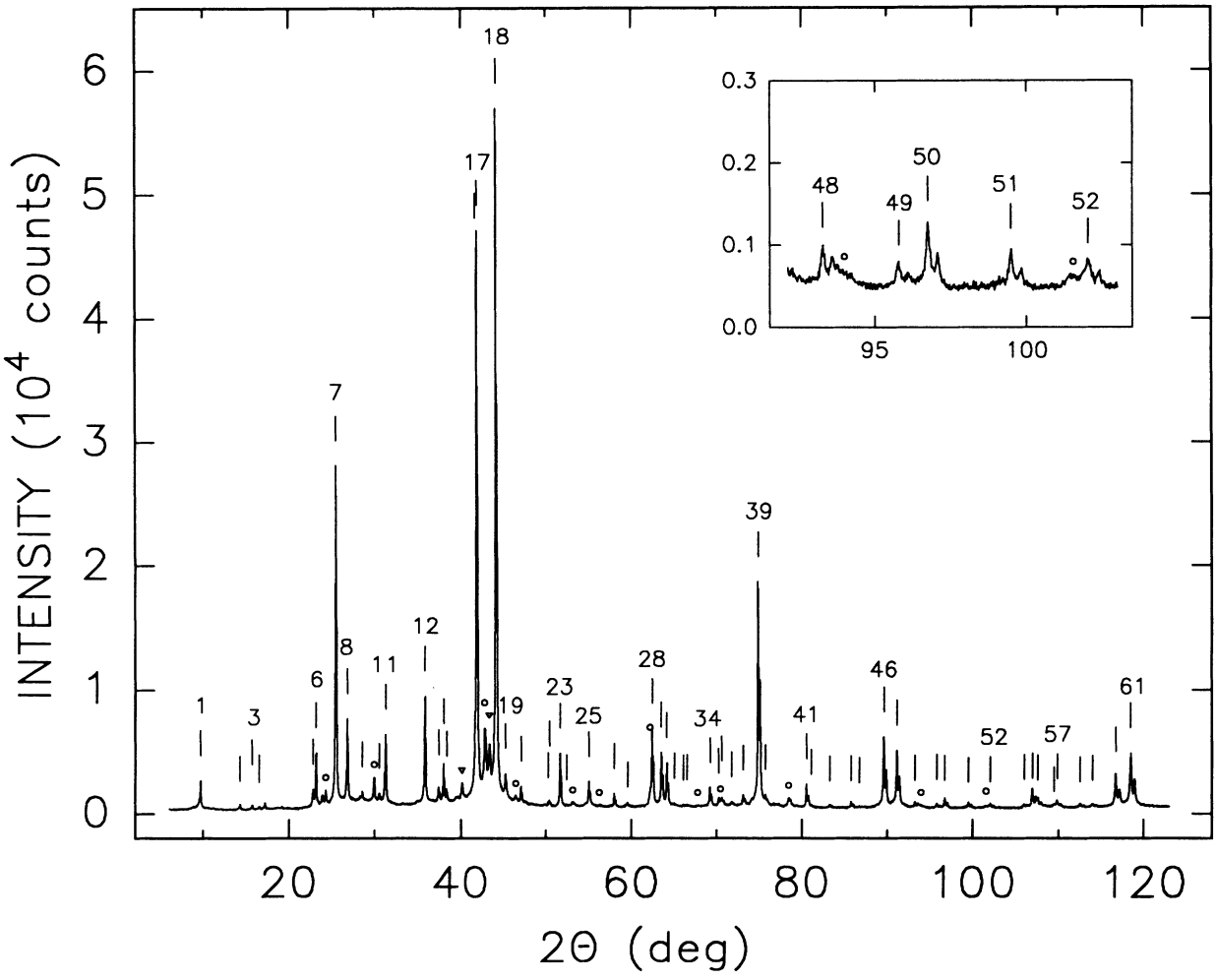

FIG. 1. X-ray-diffraction spectrum of an $Al_{70}Pd_{20}Mn_{10}$ alloy. For clarity, only some of the detected *i* peaks are labeled with integers and the vertical lines above all detected *i* peaks correspond to the positions calculated for the Cu $K\alpha_1$ radiation, as described in the text. Notice the splitting of diffraction peaks for larger 2Θ values due to $K\alpha_2$ radiation. The position, full width at half maximum, and relative intensity of each detected *i* peak determined from the fit (Ref. 50) are given in Table I together with the corresponding index. The symbols (○) and (▽) indicate the peak positions corresponding, respectively, to the strongest peaks of the hexagonal Al_3Pd_2 and decagonal Al_4Mn second phases. The inset shows a part of the spectrum with low-intensity peaks.

TABLE I. Position in terms of $2\Theta_1$ (in degrees) corresponding to Cu $K\alpha_1$ radiation and Q_{expt} (in Å^{-1}), full width at half maximum Γ_0 (in Å^{-1}), and relative intensity INT normalized to 100.0 of all detected i peaks, which are labeled with consecutive integers in column 1, as obtained from the fit (Ref. 50). The integers correspond to the vertical lines in Fig. 1. Q_{calc} (in Å^{-1}) is the calculated Q value by taking the line number 17 as the reference line. $I1$ and $I2$ are the indexes (N/M) and $(h/h',k/k',l/l')$ based on the indexing scheme of Cahn *et al.* (Ref. 51), whereas $I3$ and $I4$ are the indexes corresponding, respectively, to the indexing schemes of Elser (Ref. 52) and Bancel *et al.* (Ref. 53). The symbol $n_1n_2n_3n_4n_5n_6/2$ in the $I3$ and $I4$ schemes is an abbreviation for the index $(n_1/2)(n_2/2)(n_3/2)(n_4/2)(n_5/2)(n_6/2)$. The fcc superlattice lines are those for which $N=4n+3$ in the $I1$ scheme and which have the indexes in the form $n_1n_2n_3n_4n_5n_6/2$ in the $I3$ and $I4$ schemes.

Label	$2\Theta_1$	Q_{expt}	Q_{calc}	Γ_Q	INT	$I1$	$I2$	$I3$	$I4$
1	9.692	0.689	0.688	0.006	3.0	2/1	011000	100000	$21\bar{1}\bar{1}\bar{1}1$
2	14.269	1.013	1.013	0.010	0.6	3/3	101100	$11111\bar{1}/2$	$331\bar{1}31/2$
3	15.688	1.113	1.113	0.009	0.5	3/4	011100	$111111/2$	$31\bar{1}\bar{1}\bar{1}1/2$
4	16.503	1.171	1.170	0.010	0.3	4/4	000200	110000	$2200\bar{1}1$
5	22.818	1.614	1.614	0.008	1.6	7/8	112100	$31111\bar{1}/2$	$53\bar{1}\bar{1}33/2$
6	23.172	1.638	1.639	0.007	6.9	6/9	011200	111000	110001
7	25.494	1.800	1.800	0.009	42.1	7/11	111200	$311111/2$	$1111\bar{1}1/2$
8	26.840	1.893	1.893	0.008	10.5	8/12	002200	111100	$1110\bar{1}0$
9	28.596	2.014	2.014	0.006	1.1	10/13	122100	111110	$221\bar{0}\bar{2}0$
10	30.514	2.146	2.147	0.015	0.9	11/15	101300	$3311\bar{1}1/2$	$53\bar{1}\bar{1}13/2$
11	31.225	2.195	2.196	0.009	8.9	11/16	011300	$331111/2$	$3311\bar{1}3/2$
12	35.749	2.504	2.504	0.009	13.7	14/21	102300	211100	$2100\bar{1}1$
13	37.359	2.612	2.612	0.009	1.8	15/23	121300	$333111/2$	$3311\bar{1}1/2$
14	37.949	2.652	2.652	0.007	5.6	15/24	112300	$3331\bar{1}1/2$	$111111/2$
15	38.312	2.677	2.677	0.008	1.6	16/24	222200	211110	$210\bar{1}\bar{1}1$
16	41.636	2.899	2.899	0.008	4.9	19/28	013300	$333311/2$	$531\bar{1}31/2$
17	41.845	2.913	2.913	0.007	76.7	18/29	122300	211111	100000
18	44.107	3.063	3.063	0.007	100.0	20/32	002400	221001	110000
19	45.269	3.139	3.139	0.006	3.1	22/33	012410	221101	$2210\bar{1}1$
20	47.090	3.258	3.259	0.006	2.6	23/36	132300	$533111/2$	$331\bar{1}\bar{1}1/2$
21	50.227	3.462	3.462	0.006	0.6	27/40	103410	$53331\bar{1}/2$	$551\bar{1}3/2$
22	50.402	3.473	3.474	0.007	0.7	26/41	013400	222100	111101
23	51.641	3.553	3.553	0.007	8.3	27/43	113400	$533311/2$	$311\bar{1}\bar{1}1/2$
24	52.403	3.601	3.600	0.003	0.3	28/44	222400	311111	210001
25	55.034	3.769	3.768	0.009	3.6	31/48	112500	$5531\bar{1}1/2$	$53\bar{1}\bar{1}\bar{1}1/2$
26	58.025	3.956	3.956	0.009	1.7	34/53	122500	321111	220001
27	59.564	4.052	4.052	0.009	0.3	35/56	013500	$553113/2$	$3111\bar{1}1/2$
28	62.420	4.227	4.227	0.007	10.9	38/61	233400	322101	111000
29	63.492	4.292	4.292	0.007	8.6	39/63	123500	$5551\bar{1}1/2$	$11111\bar{1}/2$
30	64.149	4.331	4.331	0.007	6.4	40/64	242400	322111	111100
31	65.035	4.385	4.386	0.004	0.3	42/65	104500	322200	$310\bar{1}\bar{1}1$
32	66.091	4.448	4.448	0.006	0.2	43/67	333400	$733331/2$	$5311\bar{1}3/2$
33	66.498	4.472	4.472	0.008	0.2	43/68	114500	$5553\bar{1}1/2$	$3331\bar{1}1/2$
34	69.197	4.632	4.631	0.008	2.9	46/73	013600	332001	$2110\bar{1}0$
35	70.209	4.691	4.691	0.007	1.1	47/75	113600	$753113/2$	$331\bar{1}\bar{1}\bar{1}/2$
36	70.587	4.713	4.713	0.013	1.0	47/76	233500	$733333/2$	$111\bar{1}1\bar{1}/2$
37	71.702	4.777	4.777	0.012	0.4	50/77	213600	332111	320002
38	73.071	4.856	4.856	0.008	1.4	51/80	134500	$7551\bar{1}1/2$	$531\bar{1}\bar{1}3/2$
39	74.828	4.956	4.956	0.008	32.9	52/84	004600	332002	101000
40	75.654	5.002	5.003	0.005	0.9	54/85	253400	422111	221101
41	80.535	5.272	5.273	0.007	3.1	59/95	343500	$755313/2$	$311111/2$
42	81.144	5.305	5.305	0.003	0.3	60/96	224600	422211	$210\bar{1}00$
43	83.281	5.420	5.420	0.008	0.5	63/100	253500	$755333/2$	$5311\bar{1}1/2$
44	85.802	5.553	5.552	0.009	0.8	66/105	104700	432002	$2111\bar{1}1$
45	86.759	5.602	5.602	0.006	0.2	67/107	014701	$775113/2$	$3331\bar{1}\bar{1}/2$
46	89.614	5.748	5.748	0.008	10.6	70/113	124700	432112	110010
47	91.157	5.826	5.826	0.007	8.5	72/116	244600	433101	200000
48	93.282	5.931	5.931	0.007	0.8	75/120	015700	$955313/2$	$511\bar{1}\bar{1}1/2$
49	95.797	6.052	6.052	0.010	0.5	78/125	344601	433201	211001
50	96.751	6.097	6.098	0.008	1.4	79/127	125700	$955333/2$	$331\bar{1}11/2$
51	99.492	6.225	6.226	0.009	0.7	83/132	334700	$975113/2$	$531113/2$
52	102.036	6.341	6.341	0.009	0.5	86/137	364500	443101	310001
53	106.015	6.515	6.513	0.012	0.5	90/145	015800	522222	111110

TABLE I. (*Continued*).

Label	$2\Theta_1$	Q_{expt}	Q_{calc}	Γ_Q	INT	$I1$	$I2$	$I3$	$I4$
54	106.975	6.556	6.556	0.009	2.7	91/147	115800	975115/2	$311\bar{1}1\bar{1}/2$
55	107.589	6.582	6.582	0.009	1.2	92/148	115801	443102	211000
56	109.452	6.659	6.659	0.016	0.4	95/151	355600	977311/2	$533\bar{1}3\bar{1}/2$
57	109.836	6.675	6.675	0.009	0.7	95/152	125810	$977\bar{3}1/2$	$531\bar{1}1\bar{1}/2$
58	112.517	6.783	6.783	0.008	0.5	98/157	225801	533211	221000
59	113.949	6.839	6.839	0.005	0.4	99/160	354700	977313/2	$31111\bar{1}/2$
60	116.714	6.944	6.944	0.008	4.6	102/165	235800	$4441\bar{1}1$	101010
61	118.464	7.009	7.008	0.008	7.8	104/168	464600	533212	111010

corrections have to be taken into account. All our PES spectra presented here were corrected first for the energy dependence of the electron transmission of the electron energy analyzer. It was assumed that the transmission of the analyzer, including the retarding lens system, is inversely proportional to the kinetic energy of the electrons, as has been shown by Helmer *et al.*[55] Next, the PES spectra were normalized for the photon flux, and the secondary-electron contribution was subtracted in the usual way[56] by assuming that secondary-electron background intensity at each binding energy (BE) is proportional to the total integrated signal at lower binding energies. The first two corrections slightly change the shape of the original spectrum, whereas the third one produces the largest changes. Their importance is illustrated in Fig. 2. It can be seen that the corrections have no significant influence on the shape of the spectrum close to E_F, but change the spectrum substantially at higher binding energies (the negative value of BE in Fig. 2 indicates the energy scale below E_F). The PES spectra corrected in such a way can be compared not only with respect to their shape but also in terms of their intensities.

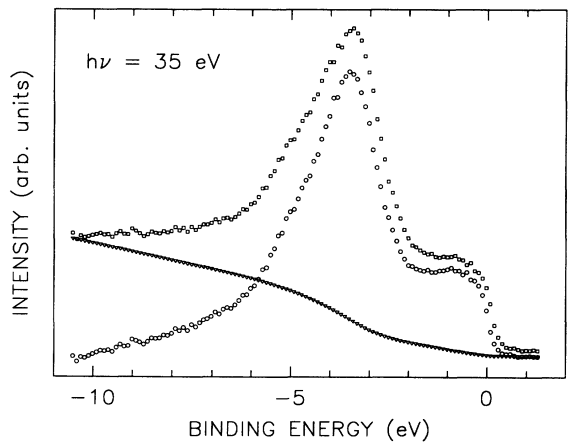

FIG. 2. Effect of the secondary-electron contribution on the valence-band spectrum of *i*-$Al_{70}Pd_{20}Mn_{10}$ measured with a photon energy $h\nu=35$ eV. (□) the analyzer- and flux-corrected original spectrum; (▽), secondary-electron contribution to the analyzer- and flux-corrected original spectrum; (○), resultant spectrum after subtraction of the secondary-electron contribution.

C. Photoemission spectroscopy data

The structure of the valence band of *i*-$Al_{70}Pd_{20}Mn_{10}$ (Fig. 2) consists of two broad features: a peak at BE≈ -1.0 eV and another one at BE$=-3.6$ eV. The BE$=-3.6$ eV feature has a shoulder on the higher BE side. There is also some weak spectral weight below BE$=-6$ eV. The features at BE$=-1.0$ and -3.6 eV must be predominantly due to the Mn $3d$ and the Pd $4d$ states because the Al sp spectral contribution is expected to be much smaller due to the small photoionization cross section for Al sp orbitals for the photon energies used here.[57] In order to identify unambiguously the origin of these two features, photoemission spectra were measured at different photon energies.

1. Resonant photoemission data

To establish the main features in a valence band due to the Mn $3d$ states, a resonant photoemission effect can be employed.[58] In this effect the ionization cross section of an outer-shell electron is enhanced as the excitation energy exceeds the threshold of an inner excitation. For TM elements the resonance occurs at excitation energies near the $3p$ threshold, which for the Mn $3p\rightarrow 3d$ transition occurs at about 47 eV. Resonance photoemission for Mn-containing alloys involves two processes. One process is the direct excitation

$$3p^6 3d^5 + h\nu \rightarrow 3p^6 3d^4 \varepsilon_f \ . \tag{1}$$

The other involves a $3p$ core excitation and a super-Coster-Kronig decay

$$3p^6 3d^5 + h\nu \rightarrow 3p^5 3d^6 \rightarrow 3p^6 3d^4 \varepsilon_f \ . \tag{2}$$

The final states obtained via these two processes are indistinguishable, so that there is a quantum interference between the two processes. As a result, the Mn $3d$ derived features are enhanced or suppressed as the photon energy is swept through the $3p$-$3d$ threshold. It can be seen in Fig. 3 that, as the photon energy increases, the intensity of the BE$=-1.0$ eV feature is slightly suppressed at $h\nu=47$ eV. This indicates that this feature may be predominantly due to the Mn $3d$-derived states.

Additional and more convincing evidence for ascribing the BE$=-1.0$ eV feature to the predominantly Mn $3d$-derived states can be obtained by performing a resonance photoemission experiment in the so-called constant-

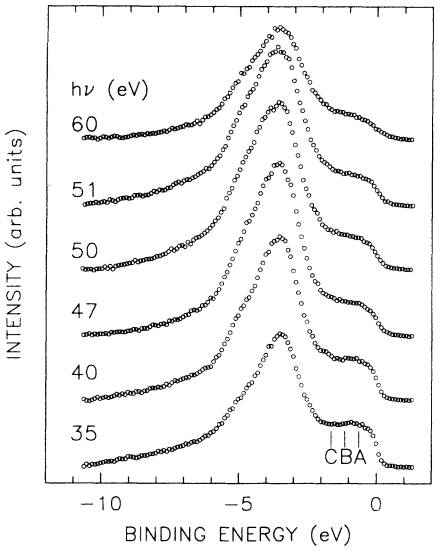

FIG. 3. Valence-band spectra of i-$Al_{70}Pd_{20}Mn_{10}$ for different photon energies around the Mn $3p \rightarrow 3d$ transition. A, B, and C identify positions for which CIS spectra were measured (Fig. 4).

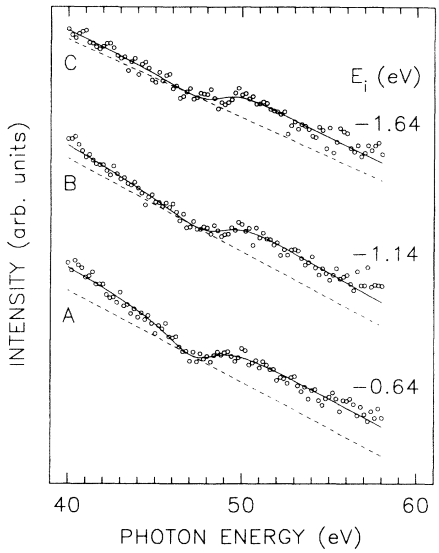

FIG. 4. Constant-initial-state (CIS) spectra for the valence-band positions A, B, and C in Fig. 3 that are identified here by the same letters and by their corresponding initial energies E_i. The solid line is a fit to the Fano profile and a linear background (shown by a dashed line), as described in the text and with parameters given in Table II.

initial-state (CIS) mode.[58,59] The photoemission intensity in this mode is measured as a function of photon energies for selected valence-band positions identified by their initial energy E_i. Such CIS spectra for the E_i values corresponding to the positions denoted by A, B, and C in Fig. 3 are shown in Fig. 4. One can clearly see the presence of resonances for photon energies around 47 eV. The line shape of the resonance resulting from the processes (1) and (2), $I(h\nu)$, can be characterized by the Fano profile[58,59]

$$I(h\nu)=I_0(\nu)\frac{(\epsilon+q)^2}{1+\epsilon^2}+I_{\rm nr}(\nu)\ , \tag{3}$$

where $I_0(\nu)$ is the nonresonant Mn $3d$ emission, $I_{\rm nr}(\nu)$ is a noninterfering background contribution, q is Fano's asymmetry parameter, and $\epsilon=2(h\nu-E_R)/\Gamma$ is the reduced energy expressed in terms of the energy, E_R, and width, Γ (FWHM), of the resonance. A linear background was assumed in the fit (dashed line in Fig. 4). The parameters obtained from the fit are given in Table II. The fitted parameters are strongly correlated and therefore caution is required in their physical interpretation. The strongest resonance occurs for $E_i=-0.64$ eV, but it is also present for other two E_i values, i.e., in the region of the valence band farther away from the E_F. The fact that the resonance takes place in a rather broad valence-band region can be interpreted as evidence of hybridization between the Mn $3d$ and the Al sp and Pd $4d$ states. This seems to be consistent with the trend of q, which diminishes with E_i (Table II). This trend, combined with the fact that a Fano line shape for small-q values shows a more pronounced dip at photon energies just below the resonance maximum (antiresonance),[58] and with the results of a theoretical model which predicts[60] that the d^{n-1} atomiclike final state in TM compounds tends to exhibit Fano-like resonances whereas the d^nL (L designates a ligand hole) final states corresponding to hybridized states show a more pronounced antiresonance behavior, seems to support the idea of hybridization between the Mn $3d$ and the Al sp and Pd $4d$ states.

The strong correlation mentioned above between the fitted parameters in Table II makes it difficult to give them a definite physical interpretation. This correlation stems from the noninterfering background $I_{\rm nr}$, which was assumed to be linear, but whose actual photon energy dependence is not known. To avoid this problem, we have generated CIS-type spectra directly from the valence-band spectra in Fig. 3 by plotting the height at a given binding energy versus the photon energy (Fig. 5). The height was calculated as an average of five height values around a given binding energy in order to remove

TABLE II. Parameters obtained by fitting the Fano line shape (3) to the CIS spectra in Fig. 4 for the E_i values corresponding to the positions A, B, and C indicated in Fig. 3.

E_i (eV)	I_0	E_R (eV)	q	Γ (eV)
−0.64	22.5(1.8)	47.5(3)	0.24(10)	3.7(6)
−1.14	15.8(1.8)	48.5(3)	0.60(12)	4.5(8)
−1.64	11.5(2.5)	48.6(5)	0.72(21)	4.0(1.2)

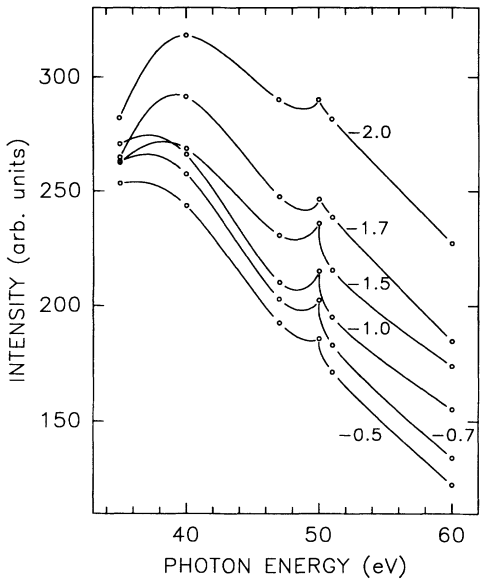

FIG. 5. CIS spectra for the indicated values of the initial energies which were calculated from the PES spectra of Fig. 3, as described in the text. The solid lines are guides for the eye.

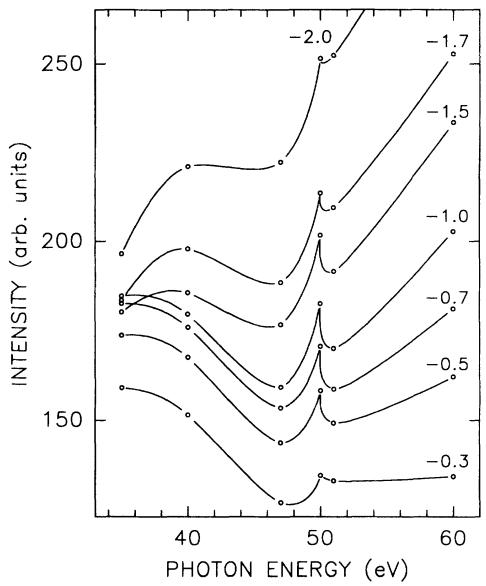

FIG. 7. CIS spectra from Fig. 5 divided by curve (*c*) from Fig. 6. An additional CIS spectrum for $E_i = -0.3$ eV, which is not shown in Fig. 5, has been added. The solid lines are guides for the eye.

possible height fluctuations due to statistical uncertainties in the measured intensity. Although there are much fewer CIS points (limited only by the number of PES spectra measured for different values of $h\nu$) in Fig. 5 as compared to Fig. 4, one can nevertheless observe clearly two effects. First, the background is nonlinear, especially for low values of $h\nu$. Second, the resonance occurs even at 2 eV below E_F and is strongest in the range 1.0–1.5 eV below E_F, which supports the earlier conclusion of the peak in the PES spectra (Figs. 2 and 3) at about 1.0 eV as being due to the Mn 3*d* derived states, and of the hybridization between the Mn 3*d* and the Al *sp* and Pd 4*d* states.

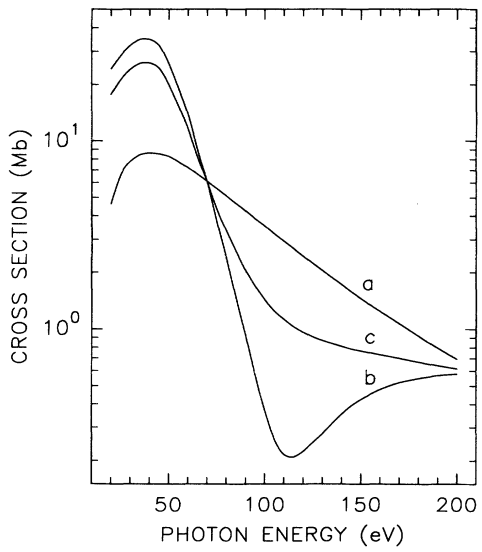

FIG. 6. Atomic subshell photoionization cross sections as a function of photon energy for Mn 3*d* (*a*) and Pd 4*d* (*b*) orbitals. Data are compiled from Ref. 57. Curve (*c*) is the weighted average of curves (*a*) and (*b*) with the weights corresponding to the Mn and Pd concentrations in $Al_{70}Pd_{20}Mn_{10}$. Note the logarithmic scale on the ordinate axis.

The shape of the CIS background in Fig. 5 is determined mainly by the photon-energy dependence of the Mn 3*d* and Pd 4*d* photoionization cross sections. To show this, we calculated the photon-energy dependence of the effective atomic Mn 3*d* and Pd 4*d* photoionization cross section corresponding to the composition $Al_{70}Pd_{20}Mn_{10}$ [curve (*c*) in Fig. 6]. Although the solid-state effects and many-body interactions may affect the detail shape of the curve (*c*) in Fig. 6, it seems reasonable to expect that its general shape will not change dramatically in the studied alloy. One can notice the relatively good agreement between the photon energy dependence of curve (*c*) in Fig. 6 and the corresponding dependence of the background of the generated CIS spectra in Fig. 5.

To correct the generated CIS spectra in Fig. 5 for the effect of the photon-energy dependence of the effective photoionization cross section, they were divided by curve (*c*) in Fig. 6. The corrected CIS spectra are shown in Fig. 7 (an additional CIS spectrum for $E_i = -0.3$ eV, which is not shown in Fig. 6, has been added). The corrected CIS spectra in Fig. 7 show more clearly than those in Fig. 5 the presence of resonances at $h\nu$ corresponding to the Mn $3p \rightarrow 3d$ transition. We interpret the occurrence of the strongest resonance for $E_i = -1.0$ eV (Fig. 7) as evidence that the feature in the valence band at 1.0(3) eV below E_F is predominantly due to the Mn 3*d*-derived states. The fact that the resonance takes place for a wide range of the E_i values (Fig. 7) indicates that the Mn 3*d* and the Al *sp* and Pd 4*d* states are hybridized. Additional experimental evidence in support of the predominantly Mn 3*d* character of the BE $= -1.0$ eV feature in the valence band of the *i*-$Al_{70}Pd_{20}Mn_{10}$ alloy will be presented in the next section.

2. *Photoemission data near the Cooper minimum*

The features in the valence bands due to the 4*d* and/or 5*d* states in alloys containing the 4*d* and/or 5*d* elements can be identified by taking advantage of the so-called Cooper minimum effect[61] which is the occurrence of a clear minimum in the photoionization cross section for particular orbitals. This effect results from the presence of a node or nodes in the radial part of the 4*d* and 5*d* (but not 3*d*) atomic wave functions. The Cooper minimum in the Pd 4*d* photoionization cross section is calculated to be at $h\nu=115$ eV for pure Pd (Ref. 57) [curve (*b*) in Fig. 6], but occurs in Pd alloys at $h\nu\approx 130$ eV.[49,61] An inspection of curves (*a*) and (*c*) in Fig. 6 shows a weak decrease of the Mn 3*d* and a dramatic decrease of the Pd 4*d* photoionization cross sections near the Cooper minimum. One can thus expect a strong suppression of the contribution of the Pd 4*d* character to the valence band of *i*-$Al_{70}Pd_{20}Mn_{10}$ for the values of $h\nu$ close to about 130 eV.

Figure 8 shows that as $h\nu$ increases from below the Cooper minimum, the relative contribution of the BE$=-3.6$ eV feature with respect to the BE$=-1.0$ eV feature first decreases, reaches a minimum at $h\nu\approx 130$ eV, and then starts to increase. Note that the Cooper minimum effect is much more dramatic (Fig. 8) than the Mn $3p\rightarrow 3d$ photoemission resonance effect (Fig. 3). It is thus concluded that the BE$=-3.6(2)$ eV feature is predominantly due to the Pd 4*d*-derived states.

One can demonstrate the occurrence of the Cooper minimum by presenting the PES spectra of Fig. 8 as difference spectra, which are shown in Fig. 9. Apart from the change of the sign of the amplitude of the broad feature at around -3.6 eV of the difference spectra caused by the Cooper minimum effect (Fig. 9), one can also notice that the Mn 3*d* feature is more clearly separated from the suppressed Pd 4*d* feature. The Mn 3*d* character in the difference spectra (Fig. 9) spreads throughout the valence band. It tends to vanish (Fig. 9)

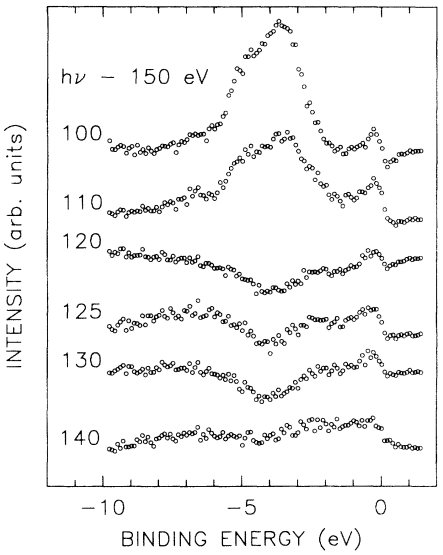

FIG. 9. Difference spectra obtained from the PES spectra in Fig. 8 by subtracting from them the spectrum measured at $h\nu=150$ eV. The numbers on the left side of each difference spectrum indicates the photon energy of the spectrum from which the $h\nu=150$ eV spectrum was subtracted.

as $h\nu$ increases because the difference between the Mn 3*d* photoionization cross section for a given $h\nu$ and the cross section at $h\nu=150$ eV decreases [Fig. 6, curve (*a*)] with increasing $h\nu$. Therefore, we conclude that, within the uncertainty of 0.3 eV, the position of the maximum of the peak of the Mn 3*d*-derived states is at BE$=-1.0$ eV and that these states extend deep below E_F due to the hybridization with the Al *sp* and/or Pd 4*d* states.

3. *Al 2p chemical shift*

The Al 2*p* core level lines in Al metal and in *i*-$Al_{70}Pd_{20}Mn_{10}$ are compared in Fig. 10. It can be noticed

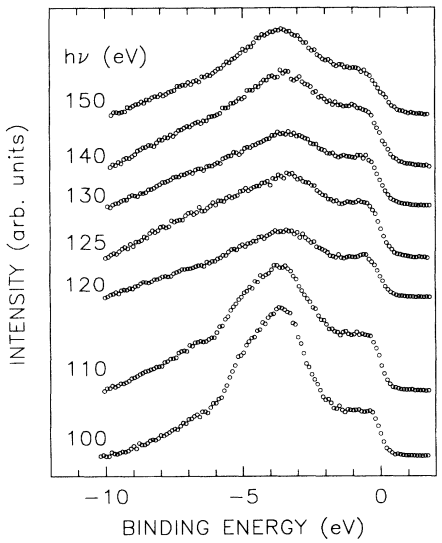

FIG. 8. Valence-band spectra of *i*-$Al_{70}Pd_{20}Mn_{10}$ for different photon energies in the vicinity of the Pd 4*d* Cooper minimum.

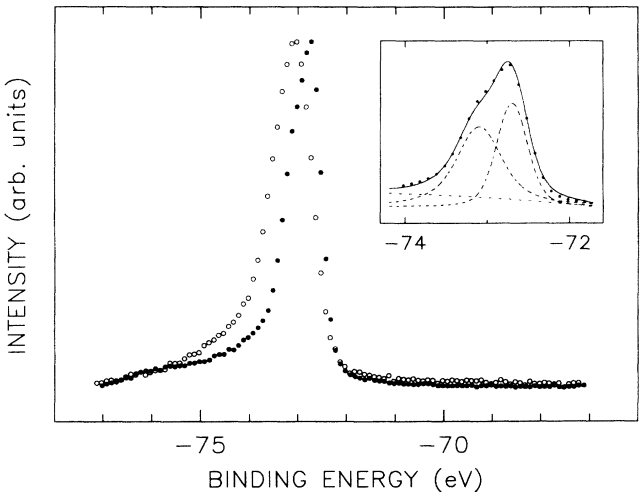

FIG. 10. Al 2*p* photoemission spectra of the Al metal (●) and *i*-$Al_{70}Pd_{20}Mn_{10}$ alloy (○). The spectra were normalized to give a constant height between the maximum and minimum recorded count. The inset shows the fit of the Al 2*p* spectrum of the Al metal with two component Voigt lines, which are also shown, corresponding to Al $2p_{1/2}$ and $2p_{3/2}$ core levels.

that the Al $2p_{1/2}$ and $2p_{3/2}$ are separated in the Al metal (inset in Fig. 10), but they overlap in the *i*-$Al_{70}Pd_{20}Mn_{10}$ alloy. The separation of the Al $2p_{1/2}$ and $2p_{3/2}$ components in the Al metal found from the fit with the two Voigt lines (inset in Fig. 10) is 0.40(13) eV, which is in a good agreement with the value of 0.42 eV reported in the literature.[62] The observation of the Al $2p_{1/2}$ and $2p_{3/2}$ lines in the Al metal confirms that the overall energy resolution of the recorded PES spectra is 0.4 eV. The main result obtained from Fig. 10 is the observation of the BE shift in *i*-$Al_{70}Pd_{20}Mn_{10}$ by 0.27(10) eV towards higher absolute BE values with respect to Al metal.

D. Discussion of the photoemission results

Our result for the position of the maximum of the Pd 4*d*-derived states at $-3.6(2)$ eV agrees well with the value of -3.5 eV obtained in a recent SXE study[45] of *i*-$Al_{71}Pd_{19}Mn_9$ (Fig. 2 in Ref. 45). Also the peak position of the Mn 3*d*-derived states at -1.3 eV (Fig. 2 in Ref. 45) agrees well with our value of $-1.0(3)$ eV. However, the Mn 3*d*-derived states are spread wider (Fig. 9) than suggested by the SXE results.[45] SXE studies of *i*-$Al_{71}Pd_{19}Mn_9$ (Ref. 45) and *i*-$Al_{70}Pd_{21}Mn_9$ (Ref. 47) show the existence of the peak in the intensity associated with the Al *s* states and the large intensity associated with the Al *p* states at about 6 eV below E_F. Therefore, we can ascribe the weak spectral weight below BE$=-6$ eV observed in the valence band of the studied sample (Fig. 2) to the Al *sp*-derived states. This spectral weight could be also caused by surface oxidation,[34] but this possibility can be excluded as the surface cleanliness was carefully monitored in the course of the PES experiments.

It is well established from experiments in the XPS and UPS photon-energy range that in pure Pd (Ref. 63) and Mn (Ref. 64) there is a high DOS(E_F). Depending on the photon energy used, the observed broad peak in the valence band of Pd lies in the range 1.3–2.3 eV below E_F (Ref. 63 and Fig. 11). For pure Mn, two features at about 0.5–1.0 and 3.0 eV below E_F are present in the valence band.[64] The presence of the Pd 4*d*-derived peak at -3.6 eV in the valence band of *i*-$Al_{70}Pd_{20}Mn_{10}$, as compared to the corresponding peak in a pure Pd metal (Fig. 11), clearly indicates the shift of the Pd 4*d*-derived states in the *i* alloy away from E_F. This shift should lead to the decrease in the Pd 4*d* contribution to the DOS(E_F). Such a shift is also observed in the valence bands of crystalline Al_3Pd and AlPd alloys (Fig. 11) and it clearly leads to a decrease in the Pd 4*d* contribution to the DOS(E_F) (Fig. 11). A similar shift of the Mn 3*d*-derived states cannot be seen in the recorded spectra (Figs. 2, 3, 8, and 9).

The depression of intensity as the energy approaches E_F observed in the PES (Refs. 34 and 39) and SXE (Refs. 42, 43, and 45–47) spectra of the QC's containing TM elements has been interpreted as evidence for the opening of a theoretically predicted[9,10] pseudogap at E_F. It should be kept in mind, however, that there are at least two effects which lead to the intensity decrease as the energy approaches E_F. The first one is a simple Fermi cutoff, which would be especially important for the QC's

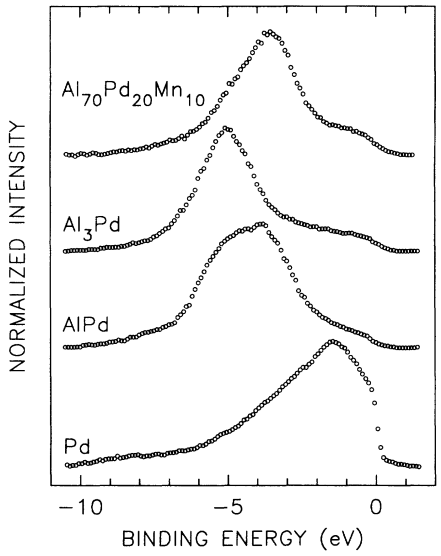

FIG. 11. Comparison of the PES valence band of *i*-$Al_{70}Pd_{20}Mn_{10}$ measured at $h\nu=60$ eV with that of a Pd metal measured also at $h\nu=60$ eV (the raw PES spectrum of Pd metal was kindly provided by Nahm and Oh; the secondary-electron contribution was subtracted from the original spectrum) and with the XPS valence bands of Al_3Pd and AlPd crystalline alloys from Fig. 12 of Ref. 65 (the secondary-electron contribution was subtracted from the original spectra). The spectra were normalized to give a constant height between the maximum and minimum recorded count.

with TM elements whose *d* states significantly contribute to the measured intensity around E_F. In the case of the studied *i*-$Al_{70}Pd_{20}Mn_{10}$, the Mn 3*d*-derived states must contribute to the measured intensity at E_F because of the closeness of the feature due to the Mn 3*d* states to E_F. The second effect leading to the decrease of intensity as the energy approaches E_F could be associated with the opening of a pseudogap at E_F. We are only able to conclude that our photoemission data are indicative of a possible opening of a pseudogap at E_F in *i*-$Al_{70}Pd_{20}Mn_{10}$, but they do not prove its existence.

If one compares the valence band of *i*-$Al_{70}Pd_{20}Mn_{10}$ measured at $h\nu=100$ eV with the corresponding band of another thermodynamically stable *i* alloy containing a transition metal, *i*-$Al_{65}Cu_{20}Fe_{15}$ (Fig. 12), one can notice two common characteristics: first, the Pd 4*d*- and Cu 3*d*-derived features are pushed away from E_F in comparison to their positions in pure Pd and Cu elements; second, the Mn and Fe 3*d*-derived states remain very close to E_F. Furthermore, the rate of the intensity decrease towards E_F is the same for both alloys (Fig. 12). It has been argued based on SXE and SXA data[43–47] that there is a pseudogap at E_F in *i*-Al-Cu-Fe alloys. If one assumes that this is indeed the case, then the observed similar intensity decrease as the energy approaches E_F observed in *i*-$Al_{65}Cu_{20}Fe_{15}$ and *i*-$Al_{70}Pd_{20}Mn_{10}$ (Fig. 12) also suggests the presence of such a pseudogap in *i*-$Al_{70}Pd_{20}Mn_{10}$.

In order to resolve the problem of a possible pseudogap around E_F in *i*-$Al_{70}Pd_{20}Mn_{10}$, high-resolution PES and

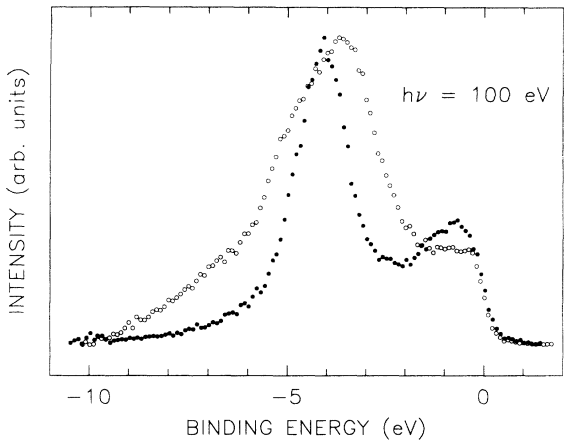

FIG. 12. Valence bands of i-$Al_{70}Pd_{20}Mn_{10}$ (○) and i-$Al_{65}Cu_{20}Fe_{15}$ (●) measured at $h\nu = 100$ eV. The raw spectrum of i-$Al_{65}Cu_{20}Fe_{15}$ from Ref. 34 has been corrected for the energy dependence of the electron transmission of the electron energy analyzer, normalized for the photon flux, and corrected for the secondary-electron background. The spectra were normalized to give a constant height between the maximum and minimum recorded count.

IPES experiments are required because only such experiments can provide information on the total (i.e., due to s, p, and d character) contribution to the, respectively, occupied and unoccupied DOS around E_F. The IPES experiments performed on i-$Al_{55}Li_{35.8}Cu_{9.2}$ (Ref. 40) revealed the opening of a pseudogap just above E_F. Electronic structure calculations performed for an approximant of i-$Al_{70}Pd_{20}Mn_{10}$ and/or a corresponding ternary crystalline alloy would be very helpful in settling the problem of a possible pseudogap around E_F in this alloy.

It is instructive to compare the valence band of the studied alloy with the bands of some crystalline Al-Pd alloys (Fig. 11). One can notice that both the positions and the widths of the Pd 4d-derived features are very similar for i-$Al_{70}Pd_{20}Mn_{10}$ and crystalline AlPd. Based on the Al and Pd content in i-$Al_{70}Pd_{20}Mn_{10}$, one would expect to observe some similarity between the valence bands of i-$Al_{70}Pd_{20}Mn_{10}$ and of crystalline Al_3Pd rather than of crystalline AlPd. The comparison presented in Fig. 11 thus suggests that i-$Al_{70}Pd_{20}Mn_{10}$ and crystalline AlPd have similar electronic structures.

Theoretical calculations[10] suggest the presence of many spikes of width less than 0.05 eV in the DOS of QC's which, along with a pseudogap at E_F, are believed to be an electronic signature of quasiperiodicity. The existence of such rapidly varying DOS has also been suggested[66] in order to explain the unusual temperature dependence of resistivity and thermoelectric power in α-Al-Mn-Si approximant. The valence bands of i-$Al_{70}Pd_{20}Mn_{10}$ presented here show no evidence for the presence of such spikes within the energy resolution of the experiment. These spikes have also not been seen in PES, IPES, SXE, and SXA experiments performed so far on other QC's,[34–47] which can be explained by the relatively low experimental energy resolution (typically 0.4 eV). However, theory also predicts[10] that the spikes are very dense. If one assumes that individual narrow spikes in the DOS of QC's cannot be observed experimentally due to the relatively low experimental energy resolution, which was worse than 0.14 eV in the experiments performed so far,[34–47] then the predicted large density of these spikes, after broadening produced by the finite resolution of the experiment, should lead to the presence of additional features in the valence bands of QC's which should not be present in the corresponding crystalline and/or amorphous counterparts. No such additional features were observed in this work and in other experiments.[34–48] In fact, the valence and conduction bands of QC's studied experimentally[34–48] are similar to the bands of the corresponding crystalline alloys.

There are only a few reports of shifts of the core-level lines in QC's with respect to pure elements and/or to other crystalline alloys.[67] Ederer *et al.*[37] reported the chemical shifts of 0.2 eV between the Al-Mn alloys of different crystal structure and pure Al, and of less than 0.1 eV between the Al-Mn alloys of crystalline and icosahedral structure. Matsubara *et al.*[40] found a 0.4-eV shift of the Al 2p and Li 1s lines towards higher absolute BE values in i-$Al_{55}Li_{35.8}Cu_{9.2}$ with respect to the Frank-Kasper crystalline alloy $Al_{54}Li_{36.8}Cu_{9.2}$. The absolute BE shift of the Al 2p line with respect to a pure Al metal observed in this paper is 0.27(10) eV (Fig. 10). The values of the observed shifts are small and are comparable to those observed in crystalline alloys.[68] The interpretation of the BE shift is complicated by the fact that it consists of contributions due to chemical, configuration, and relaxation shifts.[67] These contributions are difficult to evaluate theoretically even for simple binary alloys.[67] The minimum statement that can be made on the basis of the observed shift of the Al 2p lines in i-$Al_{70}Pd_{20}Mn_{10}$ is that the Al environment in the studied i alloy is more stable than that in pure Al. A similar conclusion was obtained by Matsubara *et al.*[40]

IV. CONCLUSIONS

The structure of the valence band of i-$Al_{70}Pd_{20}Mn_{10}$ consist of two main features at about 1.0 and 3.6 eV below E_F. The first feature was shown to be due to the Mn 3d-derived states, whereas the other was shown to result from the predominantly Pd 4d-derived states. The weak spectral weight at binding energies lower than 6 eV was ascribed to the Al sp-derived states. The strong decrease of intensity as the energy approaches E_F was interpreted as indicative of the presence of the minimum of the DOS at E_F. It was indicated, however, that high-resolution experiments probing the DOS below and above E_F are required to unambiguously determine the possible presence of such a pseudogap in a quasicrystal. The unusual features predicted by theory in the valence band, which could be associated with the quasiperiodic nature of the sample studied, were not found within the energy resolution of the experiment.

ACKNOWLEDGMENTS

This work was supported by the Natural Sciences and Engineering Research Council of Canada and a Grant-in-Aid for Scientific Research from the Ministry of Edu-

cation, Science, and Culture of Japan. The research was carried out (in part) at the National Synchrotron Light Source, Brookhaven National Laboratory, which is supported by the U.S. Department of Energy, Division of Materials Sciences and Division of Chemical Sciences (DOE Contract No. DE-AC02-76CH00016). Two of us (G.W.Z. and Z.M.S.) are deeply indebted to Dr. M.-L. Shek for her help in conducting the PES experiments.

*Author to whom correspondence should be addressed.

[1]D. Shechtman, I. Blech, D. Gratis, and J. W. Cahn, Phys. Rev. Lett. **53**, 1951 (1984).

[2]*Quasicrystals, The State of the Art,* edited by D. P. DiVincenzo and P. J. Steinhardt (World Scientific, Singapore, 1991); *Quasicrystals,* edited by T. Fujiwara and T. Ogawa (Springer-Verlag, Berlin, 1990).

[3]S. J. Poon, Adv. Phys. **41**, 303 (1992), and references therein.

[4]A.-P. Tsai, A. Inoue, and T. Masumoto, Jpn. J. Appl. Phys. **26**, L1505 (1987); **27**, L1587 (1988).

[5]F. S. Pierce, S. J. Poon, and Q. Guo, Science **261**, 737 (1993).

[6]H. Akiyama, Y. Honda, T. Hashimoto, K. Edagawa, and S. Takeuchi, Jpn. J. Appl. Phys. **32**, L1003 (1993).

[7]T. Klein, C. Berger, D. Mayou, and F. Cyrot-Lackmann, Phys. Rev. Lett. **66**, 2907 (1991).

[8]S. Kimura and S. Takeuchi, *Quasicrystals, The State of the Art* (Ref. 2), p. 313.

[9]A. P. Smith and N. W. Ashcroft, Phys. Rev. Lett. **59**, 1365 (1987); J. Friedel and F. Dénoyer, C. R. Acad. Sci. (Paris) **305**, 171 (1987); V. G. Vaks, V. V. Kamyshenko, and G. D. Samolyuk, Phys. Lett. A **132**, 131 (1988); J. Friedel, Helv. Phys. Acta **61**, 538 (1988).

[10]T. Fujiwara, Phys. Rev. B **40**, 942 (1989); J. Non-Cryst. Solids **117-118**, 844 (1990); T. Fujiwara and H. Tsunetsugu, *Quasicrystals, The State of the Art* (Ref. 2), p. 343; T. Fujiwara and T. Yokokawa, Phys. Rev. Lett. **66**, 333 (1991); J. Hafner and M. Krajči, *ibid.* **68**, 2321 (1992); Europhys. Lett. **17**, 145 (1992); J. Non-Cryst. Solids **150**, 337 (1992); Phys. Rev. B **47**, 1179 (1993); T. Fujiwara, J. Non-Cryst. Solids **156-158**, 865 (1993).

[11]T. Klein, H. Rakoto, C. Berger, G. Fourcaudot, and F. Cyrot-Lackmann, Phys. Rev. B **45**, 2046 (1992); A. Sahnoune, J. O. Ström-Olsen, and A. Zaluska, *ibid.* **46**, 10 629 (1992); T. Klein, C. Berger, G. Fourcaudot, J. C. Grieco, P. Lanco, and F. Cyrot-Lackmann, J. Non-Cryst. Solids **156-158**, 901 (1993).

[12]H. Akiyama, T. Hashimoto, T. Shibuya, K. Edagawa, and S. Takeuchi, J. Phys. Soc. Jpn. **62**, 639 (1993); S. Takeuchi, H. Akiyama, N. Naito, T. Shibuya, K. Edagawa, and K. Kimura, J. Non-Cryst. Solids **153-154**, 353 (1993); M. A. Chernikov, A. Bernasconi, C. Beeli, and H. R. Ott, Europhys. Lett. **21**, 767 (1993).

[13]A. P. Tsai, A. Inoue, Y. Yokoyama, and T. Masumoto, Mater. Trans. Jpn. Inst. Met. **31**, 98 (1990); Philos. Mag. Lett. **61**, 9 (1990); A.-P. Tsai, Y. Yokoyama, A. Inoue, and T. Masumoto, Jpn. J. Appl. Phys. **29**, L1161 (1990).

[14]A.-P. Tsai, A. Inoue, and T. Masumoto, Philos. Mag. Lett. **62**, 95 (1990).

[15]A.-P. Tsai, Y. Yokoyama, A. Inoue, and T. Masumoto, J. Mater. Res. **6**, 2646 (1991); K. Edagawa, A. Waseda, H. Morioka, and H. Ino (unpublished); A. P. Tsai, H. S. Chen, A. Inoue, and T. Masumoto, Phys. Rev. B **43**, 8782 (1991); M. De Boissieu, M. Durand-Charre, P. Bastie, A. Carabelli, M. Boudard, M. Bessiere, S. Lefebvre, C. Janot, and M. Audier, Philos. Mag. Lett. **65**, 147 (1992); C. Janot, M. De Boissieu, M. Boudard, H. Vincent, M. Durand, J. M. Dubois, and C. Dong, J. Non-Cryst. Solids **150**, 322 (1992); A. P. Tsai, Y. Yokoyama, A. Inoue, and T. Masumoto, *ibid.* **150**, 327 (1992); A. P. Tsai, H. S. Chen, A. Inoue, and T. Masumoto, Jpn. J. Appl. Phys. **31**, L419 (1992); S. W. Kycia, A. I. Goldman, T. A. Lograsso, D. W. Delaney, M. Sutton, E. Dufresne, R. Brüning, and B. Rodricks, Phys. Rev. B **48**, 3544 (1993).

[16]C. Dong, J. M. Dubois, M. De Boissieu, M. Boudard, and C. Janot, J. Mater. Res. **6**, 2637 (1991); M. Boudard, M. De Boissieu, C. Janot, J. M. Dubois, and C. Dong, Philos. Mag. Lett. **64**, 197 (1991); M. Boudard, M. De Boissieu, C. Janot, G. Heger, C. Beeli, H.-U. Nissen, H. Vincent, R. Ibberson, M. Audier, and J. M. Dubois, J. Phys.: Condens. Matter **4**, 10 149 (1992); M. Boudard, M. De Boissieu, C. Janot, G. Heger, C. Beeli, H. U. Nissen, H. Vincent, M. Audier, and J. M. Dubois, J. Non-Cryst. Solids **153-154**, 5 (1993).

[17]A. Sadoc and J. M. Dubois, J. Non-Cryst. Solids **153-154**, 83 (1993).

[18]M. Tanaka (unpublished); C. Beeli, H.-U. Nissen, and J. Robadey, Phil. Mag. Lett. **63**, 87 (1991); K. Hiraga and W. Sun, J. Phys. Soc. Jpn. **62**, 1833 (1993); Philos. Mag. Lett. **67**, 117 (1993); M. Wollgarten, H. Lakner, and K. Urban, *ibid.* **67**, 9 (1993); N. Menguy, M. Audier, M. De Boissieu, P. Guyot, M. Boudard, and C. Janot, *ibid.* **67**, 35 (1993); J. Feng, R. Wang, and Z. Wang, *ibid.* **68**, 321 (1993); M. Audier, M. Durand-Charre, and M. De Boissieu, Philos. Mag. B **68**, 607 (1993); T. L. Daulton and K. F. Kelton, *ibid.* **68**, 697 (1993).

[19]K. Fukamichi and T. Goto (unpublished); K. Fukamichi, T. Kikuchi, Y. Hattori, A. P. Tsai, A. Inoue, T. Masumoto, and T. Goto, in *Quasicrystals,* edited by K. H. Kuo and T. Ninomiya (World Scientific, Singapore, 1991), p. 256.

[20]P. Lanco, T. Klein, C. Berger, F. Cyrot-Lackmann, G. Fourcaudot, and A. Sulpice, Europhys. Lett. **18**, 227 (1992); P. Lanco, C. Berger, F. Cyrot-Lackmann, and A. Sulpice, J. Non-Cryst. Solids **153-154**, 325 (1993).

[21]S. Matsuo, H. Nakano, T. Ishimasa, and M. Mori, J. Phys. Soc. Jpn. **62**, 4044 (1993).

[22]M. A. Chernikov, A. Bernasconi, C. Beeli, A. Schilling, and H. R. Ott, Phys. Rev. B **48**, 3058 (1993).

[23]Z. M. Stadnik, Hyperfine Interact. (to be published).

[24]M. E. McHenry, M. E. Eberhart, R. C. O'Handley, and K. H. Johnson, Phys. Rev. Lett. **56**, 81 (1986).

[25]R. C. O'Handley, R. A. Dunlap, and M. E. McHenry, in *Handbook of Magnetic Materials,* edited by K. H. J. Buschow (Elsevier, Amsterdam, 1991), Vol. 6, p. 453.

[26]V. De Coulon, F. A. Reuse, and S. N. Khanna, Phys. Rev. B **48**, 814 (1993); F. Liu, S. N. Khanna, L. Magaud, P. Jena, V. De Coulon, X.-G. He, and F. Cyrot-Lackman, Phys. Rev. B **48**, 1295 (1993).

[27]Z. M. Stadnik, G. Stroink, H. Ma, and G. Williams, Phys. Rev. B **39**, 9797 (1989), and references therein.

[28]T. Shinohara, A. P. Tsai, and T. Masumoto, J. Phys.: Condens. Matter **4**, 3043 (1992); T. Shinohara and T. Sato, Sci. Rep. Res. Inst. Tohoku Univ. A **38**, 34 (1993); T. Shinohara, A. P. Tsai, T. Masumoto, and T. Sato, Mater. Trans. Jpn. Inst. Met. **34**, 146 (1993).

[29]J.-B. Suck, J. Non-Cryst. Solids **153-154**, 573 (1993); M. De Boissieu, M. Boudard, R. Bellissent, M. Quilichini, B. Hennion, R. Currat, A. I. Goldman, and C. Janot, J. Phys.: Condens. Matter **5**, 4945 (1993).

[30]H. Nakajima, J. Asai, K. Nonaka, I. Shinbo, A. P. Tsai, and T. Masumoto, Philos. Mag. Lett. **68**, 315 (1993).
[31]A. P. Tsai, H. Suenaga, M. Ohmori, Y. Yokoyama, A. Inoue, and T. Masumoto, Jpn. J. Appl. Phys. **31**, 2530 (1992).
[32]Y. Yokoyama, T. Miura, A.-P. Tsai, A. Inoue, and T. Masumoto, Mater. Trans. Jpn. Inst. Met. **33**, 97 (1992).
[33]L. Degiorgi, M. A. Chernikov, C. Beeli, and H. R. Ott, Solid State Commun. **87**, 721 (1993).
[34]Z. M. Stadnik and G. Stroink, Phys. Rev. B **47**, 100 (1993), and references therein.
[35]A. Traverse, L. Dumoulin, and E. Belin, in *Quasicrystalline Materials,* edited by Ch. Janot and J. M. Dubois (World Scientific, Singapore, 1988), p. 399.
[36]P. A. Bruhwiler, J. L. Wagner, B. D. Biggs, Y. Shen, K. M. Wong, S. E. Schnatterly, and S. J. Poon, Phys. Rev. B **37**, 6529 (1988).
[37]D. L. Ederer, R. Schaefer, K.-L. Tsang, C. H. Zhang, T. A. Caliicott, and E. T. Arakawa, Phys. Rev. B **37**, 8594 (1988).
[38]E. Belin and A. Traverse, J. Phys.: Condens. Matter **3**, 2157 (1991).
[39]M. Mori, S. Matsuo, T. Ishimasa, T. Matsuura, K. Kamiya, H. Inokuchi, and T. Matsukawa, J. Phys.: Condens. Matter **3**, 767 (1991).
[40]H. Matsubara, S. Ogawa, T. Kinoshita, K. Kishi, S. Takeuchi, K. Kimura, and S. Suga, Jpn. J. Appl. Phys. **A30**, L389 (1991).
[41]M. Mori, K. Kamiya, S. Matsuo, T. Ishimasa, H. Nakano, H. Fijimoto, and H. Inokuchi, J. Phys.: Condens. Matter **4**, L157 (1992).
[42]E. Belin, J. Kojnok, A. Sadoc, A. Traverse, M. Harmelin, C. Berger, and J.-M. Dubois, J. Phys.: Condens. Matter **4**, 1057 (1992).
[43]E. Belin, Z. Dankhazi, A. Sadoc, Y. Calvayrac, T. Klein, and J.-M. Dubois, J. Phys.: Condens. Matter **4**, 4459 (1992).
[44]E. Belin, in *Physics and Chemistry of Finite Systems,* edited by P. Jena, S. N. Khanna, and B. K. Rao (Kluwer Academic, Amsterdam, 1992), Vol. II, p. 829.
[45]E. Belin and Z. Danhkázi, J. Non-Cryst. Solids **153-154**, 298 (1993).
[46]A. Sadoc, E. Belin, Z. Dankhazi, and A. M. Flank, J. Non-Cryst. Solids **153-154**, 338 (1993).
[47]E. Belin, Z. Dankhazi, and A. Sadoc, J. Non-Cryst. Solids **156-158**, 896 (1993).
[48]P. Häussler, Phys. Rep. **222**, 65 (1992), and references therein.
[49]H. Wright, P. Weightman, P. T. Andrews, W. Folkerts, C. F. J. Flipse, G. Sawatzky, D. Norman, and H. Padmore, Phys. Rev. B **35**, 519 (1987), and references therein.
[50]W. N. Schreiner and R. Jenkins, Adv. X-ray Anal. **26**, 141 (1983).
[51]J. W. Cahn, D. Shechtman, and D. Gratias, J. Mater. Res. **1**, 13 (1986).
[52]V. Elser, Acta Crystallogr. A **42**, 36 (1986).
[53]P. A. Bancel, P. A. Heiney, P. W. Stephens, A. I. Goldman, and P. M. Horn, Phys. Rev. Lett. **54**, 2422 (1985).
[54]J. Devaud-Rzepski, A. Quivy, Y. Calvayrac, M. Cornier-Quiquandon, and D. Gratias, Philos. Mag. B **60**, 855 (1989).
[55]J. C. Helmer and N. H. Weichert, Appl. Phys. Lett. **13**, 266 (1968).
[56]D. A. Shirley, Phys. Rev. B **5**, 4709 (1972).
[57]J. J. Yeh and I. Lindau, At. Data Nucl. Data Tables **32**, 1 (1985).
[58]L. C. Davis, J. Appl. Phys. **59**, R25 (1986), and references therein.
[59]C. Kunz, in *Photoemission in Solids II,* edited by L. Ley and M. Cardona (Springer-Verlag, Berlin, 1979), p. 299.
[60]R. J. Lad and V. E. Henrich, Phys. Rev. B **38**, 10 860 (1988).
[61]G. Rossi, I. Lindau, L. Braicovich, and I. Abbati, Phys. Rev. B **28**, 3031 (1983), and references therein.
[62]Y. Baer, G. Busch, and P. Cohn, Rev. Sci. Instrum. **46**, 466 (1975); S. A. Flodstrom, R. Z. Bachrach, R. S. Bauer, and S. B. Hagström, Phys. Rev. Lett. **37**, 1282 (1976).
[63]C. S. Fadley and D. A. Shirley, in *Electronic Density of States,* Natl. Bur. Stand. (U.S.) Spec. Publ. No. 323, edited by L. H. Bennett (U.S. GPO, Washington, D.C., 1971), p. 163; N. V. Smith, G. K. Wertheim, S. Hüfner, and M. M. Traum, Phys. Rev. B **10**, 3197 (1974); N. Mårtensson, R. Nyholm, H. Calén, J. Hedman, and B. Johansson, *ibid.* **24**, 1725 (1981).
[64]L. Ley, O. B. Dabbousi, S. P. Kowalczyk, F. R. McFeely, and D. A. Shirley, Phys. Rev. B **16**, 5372 (1977); A. Kakizaki, H. Sugawara, I. Nagakura, and T. Ishii, J. Phys. Soc. Jpn. **49**, 2183 (1980); S. Raaen and V. Murgai, Phys. Rev. B **36**, 887 (1987).
[65]J. C. Fuggle, F. U. Hillebrecht, R. Zeller, Z. Zolnierek, P. A. Bennett, and Ch. Freiburg, Phys. Rev. B **27**, 2145 (1983).
[66]B. D. Biggs, F. S. Pierce, and S. J. Poon, Europhys. Lett. **19**, 415 (1992).
[67]Z. M. Stadnik and G. Stronik, J. Non-Cryst. Solids **99**, 233 (1988), and references therein.
[68]F. U. Hillebrecht, J. C. Fuggle, P. A. Bennett, Z. Zolnierek, and Ch. Freiburg, Phys. Rev. B **27**, 2179 (1983).